Journal of Magnetic Resonance 194 (2008) 128–135

Contents lists available at ScienceDirect

Journal of Magnetic Resonance

journal homepage: www.elsevier.com/locate/jmr

The effect of impermeable boundaries of arbitrary geometry on the apparent diffusion coefficient

Astrid F. Frøhlich [a,*], Sune N. Jespersen [a], Leif Østergaard [a], Valerij G. Kiselev [b]

[a] Department of Neuroradiology, Center of Functionally Integrative Neuroscience (CFIN), University Hospital of Aarhus, Nørrebrogade 44, Building 30, 8000 Aarhus C, Denmark
[b] Medical Physics, Department of Diagnostic Radiology, University Hospital Freiburg, Freiburg, Germany

ARTICLE INFO

Article history:
Received 23 April 2008
Revised 13 June 2008
Available online 24 June 2008

Keywords:
NMR
Diffusion
Restricted diffusion
Cumulant expansion
Apparent diffusion coefficient
Biological boundaries

ABSTRACT

The apparent diffusion coefficient (ADC) obtained from NMR measurements is modelled for diffusion in a compartment restricted by an impermeable boundary. For a given pulse sequence, the ADC can be determined from the connected velocity autocorrelation function (the second-order velocity cumulant), which we show can be expressed as a double surface integral over the boundary, involving the probability for molecules to diffuse from one boundary point to another. There is no restriction on the geometry of the boundary. This result allows a fast calculation of the ADC for an arbitrary time course of the diffusion-sensitizing gradient. Explicit examples are given for diffusion within three basic geometries for different pulse sequences. The ADCs measured with the Stejskal–Tanner pulse sequence and a more realistic pulse sequence with slice selection gradient and eddy current compensation are found to yield almost identical results. The application of the results are discussed in relation to determination of the microscopic structure of brain white matter.

1. Introduction

Diffusion-weighted MRI probes cellular structure of living tissue. However, the detailed relation between the biological microstructure and the acquired MR signal is extremely complex and the study of this relation remains an area of active research.

Considerable insight into this field may be gleaned from the exploration of the structure of porous media by diffusion-weighted MRI [1–3]. In such media, an NMR visible fluid is confined in an impermeable NMR-invisible matrix. The physics underlying diffusion and the MRI signal is well understood in this context [4]. In particular, the short-time behavior of the apparent diffusion coefficient (ADC) can be related to the geometry of the matrix:

$$D = D_0\left(1 - c\cdot\sqrt{D_0 T}\frac{S}{V}\right), \tag{1}$$

where S and V are the surface and volume of the pore space, D_0 is the diffusion coefficient in the bulk fluid, T is the diffusion time, and c is a constant depending on the pulse sequence [1–3]. By virtue of the central limit theorem, the diffusion takes its free form again for long times, with a reduced ADC. The reduction is described by the so-called tortuosity, λ, defined through $D = D_0/\lambda^2$.

The diffusion-weighted signal in biological tissue is more difficult to analyze, for experimentally relevant diffusion times, since many of the simplifications applicable to porous materials do not apply. In most tissue types, NMR visible water is present inside and outside cells. Furthermore, the majority of biological membranes are penetrable for water molecules, and there are few compartments with free diffusion. For example, the medium surrounding neuronal fibers consists of glia cells and an abundance of macro-molecules, and the diffusion in such a medium is hindered. This issue was considered in Ref. [5], where a short-time expression for the ADC was derived for molecules diffusing in a heterogeneous medium with restrictive boundaries in one-dimension. No simplifying assumptions were made about the diffusion in the bulk medium. The results ruled out a simple interpretation of the diffusion-weighted signal in the spirit of Eq. (1).

The dependence of the ADC on the measurement technique presents another problem for the interpretation of the diffusion-weighted signal. In the narrow pulse approximation, with its unambiguous definition of the diffusion time and the Fourier relation between the spin displacement distribution and the NMR signal, the ADC is simply related to the mean square displacement of individual spins. However, the narrow pulse approximation is rarely achievable with the gradient systems of clinical scanners, and for the more complicated pulse sequences employed in practice, the relation of the ADC to microscopic variables is less direct. For these reasons, it is important to develop methods for the calculation of the ADCs for different realistic pulse sequences.

* Corresponding author. Fax: +45 89894400.
E-mail address: astrid@pet.auh.dk (A.F. Frøhlich).

1090-7807/$ - see front matter © 2008 Elsevier Inc. All rights reserved.
doi:10.1016/j.jmr.2008.06.009

The analysis in Ref. [5] was based on a microscopic determination of the ADC in terms of an autocorrelation function of molecular velocity (the second-order cumulant) [6]. In the present paper, we extend this approach in the context of diffusion in a homogeneous medium restricted by impermeable boundaries (hereafter referred to as a pore), to derive an expression for the second-order velocity cumulant for arbitrary pulse sequences and a three-dimensional geometry, in terms of the diffusion propagator inside the pore. We find that the second-order velocity cumulant can be expressed as a double surface integral of the diffusion propagator. This expression is related to existing expressions for the ADC, e.g., in Refs. [7,2], but the new insight makes both analytical and numerical calculations less demanding, enabling in particular the straightforward calculation of the ADC for an arbitrary form of the diffusion-sensitizing gradient pulse. The result is used to compare the ADCs found with different pulse sequences in the geometry of a slab, a cylinder and a sphere.

The paper is organized as follows: in the next section, we consider the diffusion-weighted signal at small b-values and define the ADC. We then find a three-dimensional expression for the second-order velocity cumulant which depends on the diffusion propagator at the surface only. The applicability of this expression is demonstrated in three geometries: diffusion between impermeable walls, within an impermeable cylinder and within an impermeable sphere. For these geometries, the ADC is derived and discussed for three different pulse sequences. The discussion following in Section 4 focuses on the expression found for the second-order velocity cumulant and a comparison between the ADC results for the different pulse sequences. In Appendix A, two alternative ways of achieving the expression for the second-order cumulant are briefly outlined. For convenience, expressions for the diffusion propagator in the three geometries are given in Appendix B.

2. Theory

2.1. The apparent diffusion coefficient

In the limit of a weak diffusion weighting in the imaging sequence ($b \to 0$), the normalized NMR signal, S, from a sample can be written in terms of the second-order velocity cumulant, $u^{(2)}$:

$$\ln S \approx -\frac{1}{2}\sum_{ij}\int_0^T u_{ij}^{(2)}(t_1,t_2)G_i(t_1)G_j(t_2)\,\mathrm{d}t_1\,\mathrm{d}t_2, \tag{2}$$

which is the first term in the cumulant expansion of the signal and can be obtained by partial integration of the expression given by Callaghan in Ref. [6, Chapter 6]. The summation indices i and j count the three vector components and $\mathbf{G}(t)$ is the integral of the gradient of the Larmor frequency, $\mathbf{g}(t)$, applied for the diffusion weighting:

$$\mathbf{G}(t) = \int_0^t \mathbf{g}(t_1)\,\mathrm{d}t_1 = \gamma\int_0^t \nabla B_z(t_1)\,\mathrm{d}t_1. \tag{3}$$

The condition for echo formation is $\mathbf{G}(T) = \mathbf{G}(0) = 0$. A refocusing pulse applied at a time point t_0 is taken into account by changing the sign of $g(t)$ for $t < t_0$.

The second-order velocity cumulant is an autocorrelation function

$$u_{ij}^{(2)}(t_1,t_2) = \langle v_i(t_1)v_j(t_2)\rangle - \langle v_i(t_1)\rangle\langle v_j(t_2)\rangle, \tag{4}$$

where the angular brackets denote averaging over all diffusing molecules contributing to the signal. When bulk flow is absent, the velocity cumulants depend on time differences only (stationarity), which is assumed below. In the case of free diffusion in a homogeneous medium, the second-order velocity cumulant takes the form [6], chapt. 6, [5]

$$u_{ij}^{(2)}(t_1,t_2) = 2D_0\delta_{ij}\delta(t_2-t_1). \tag{5}$$

The signal in Eq. (2) is proportional to the squared amplitude of the gradient and is often written in terms of the b-factor, defined by

$$b_{ij} = \int_0^{T_E} G_i(t)G_j(t)\,\mathrm{d}t. \tag{6}$$

The conventional definition of the diffusion tensor using Eqs. (2) and (5) implies taking the limit of small b-factors when considering diffusion in heterogeneous media. The ADC tensor, $\mathbf{D}$, is defined through

$$\ln S \simeq -\sum_{ij} b_{ij}D_{ij}, \tag{7}$$

for a small diffusion weighting. In order to determine the independent components of the ADC tensor, the signal must be measured with diffusion gradients applied along at least six non-collinear directions. The issue of calculating the diffusion tensor from the diffusion-weighted signal is discussed, e.g., in Ref. [8]. In the simple geometries considered here, the diagonalization of all tensors involved is trivial and the diffusion tensor can be found by a simple division by the eigenvalues of the b-matrix. When the diffusion weighting is applied only in one direction, e.g., the x-direction, as is assumed in the following examples, the ADC takes the form

$$D = \frac{1}{2b_{xx}}\int_0^T u_{xx}^{(2)}(t_2-t_1)G_x(t_2)G_x(t_1)\,\mathrm{d}t_1\,\mathrm{d}t_2. \tag{8}$$

The index xx on D has been omitted for ease of notation. It follows from Eq. (8) that the ADC depends on the specific shape of $G(t)$. This dependence disappears only in a homogeneous medium, where $u^{(2)}$ takes the form given in Eq. (5).

In the following we determine the second-order velocity cumulant $u^{(2)}$ in order to calculate the apparent diffusion coefficient for different pulse sequences.

2.2. Second-order velocity cumulant

In this section, we consider the second-order velocity cumulant for diffusion in three-dimensions in a pore of arbitrary geometry with reflecting boundaries.

The velocity cumulant in Eq. (8) is calculated by straightforward discretization of the derivative in the definition of velocity. Suppose that the position of all molecules is measured at a time t after which they are labelled, and the positions are measured again after an infinitesimally short time Δt. This allows calculation of the instantaneous velocities of the molecules. We define a velocity operator as

$$\mathscr{V}_i \equiv \lim_{\Delta t\to 0}\frac{r_{2i}-r_{1i}}{\Delta t}\psi(\mathbf{r}_2,\mathbf{r}_1,\Delta t), \tag{9}$$

where the diffusion propagator, ψ, is the solution to the diffusion equation,

$$\frac{\partial\psi(\mathbf{r_2},\mathbf{r_1},t)}{\partial t} = D_0\nabla^2\psi(\mathbf{r_2},\mathbf{r_1},t) \tag{10}$$

with the initial condition

$$\psi(\mathbf{r_2},\mathbf{r_1},0) = \delta^3(\mathbf{r}_2-\mathbf{r}_1) \tag{11}$$

and with the reflecting boundary condition

$$D_0\hat{\mathbf{n}}\cdot\nabla\psi(\mathbf{r_2},\mathbf{r_1},t)|_{\mathbf{r}\in\Omega} = 0, \tag{12}$$

where Ω is the surface and $\hat{\mathbf{n}}$ an outward pointing normal to the surface. For very short times, the diffusion propagator is not influenced by the boundaries and keeps its initial form, Eq. (11), and the velocity operator in Eq. (9) takes the form

$$\mathscr{V}_i = -2D_0 \frac{\partial}{\partial r_{2i}} \delta^3(\mathbf{r}_2 - \mathbf{r}_1). \tag{13}$$

This is derived by integrating the velocity operator with an arbitrary smooth function $f(\mathbf{r}_2)$. This function is expanded in a power series from which only the linear term contributes in the limit of vanishing time:

$$\begin{aligned}\int \mathscr{V}_i f(\mathbf{r}_2) d^3\mathbf{r}_2 &= \int d^3\mathbf{r}_2 \frac{(r_{2i} - r_{1i})^2}{\Delta t} \psi(\mathbf{r}_2, \mathbf{r}_1, \Delta t) \frac{\partial}{\partial r_{2i}} f(\mathbf{r}_2)|_{\mathbf{r}_2=\mathbf{r}_1} \\ &= 2D_0 \frac{\partial}{\partial r_{2i}} f(\mathbf{r}_2)|_{\mathbf{r}_2=\mathbf{r}_1},\end{aligned} \tag{14}$$

using $\langle (r_{2i} - r_{1i})^2 \rangle = 2D_0\Delta t$ at short times. This integration result proves by definition the delta-functional form given in Eq. (13). The Gaussian form of the diffusion propagator at short times determines the actual representation of the derivative of the delta-function.

The velocity autocorrelation function, $\langle v_i(t_1) v_j(t_2) \rangle$, can now be calculated in the following way, first for $t_2 - t_1 > 0$:

$$\begin{aligned}\langle v_i(t_1) v_j(t_2) \rangle = \int_V &\mathscr{V}_i(\mathbf{r}_1 - \mathbf{r}_0) \psi(\mathbf{r}_2, \mathbf{r}_1, t_2 - t_1) \mathscr{V}_j(\mathbf{r}_3 - \mathbf{r}_2) \\ &\times \frac{d\mathbf{r}_0}{V} d\mathbf{r}_1 d\mathbf{r}_2 d\mathbf{r}_3.\end{aligned} \tag{15}$$

By introducing a pore shape function $v(\mathbf{r})$ which is unity inside the pore and zero outside, the integration limits in Eq. (15) can be extended to the whole space:

$$\begin{aligned}\langle v_i(t_1) v_j(t_2) \rangle &= \frac{1}{V} \int \mathscr{V}_i(\mathbf{r}_1 - \mathbf{r}_0) \psi(\mathbf{r}_2, \mathbf{r}_1, t_2 - t_1) \mathscr{V}_j(\mathbf{r}_3 - \mathbf{r}_2) \\ &\quad \cdot v(\mathbf{r}_0) \cdots v(\mathbf{r}_3) d\mathbf{r}_0 d\mathbf{r}_1 d\mathbf{r}_2 d\mathbf{r}_3 \\ &= -\frac{4D_0^2}{V} \int \delta^3(\mathbf{r}_1 - \mathbf{r}_0) \psi(\mathbf{r}_2, \mathbf{r}_1, t_2 - t_1) \delta^3(r_3 - r_2) \\ &\quad \cdot \frac{\partial}{\partial r_{0i}} v(\mathbf{r}_0) v(\mathbf{r}_1) v(\mathbf{r}_2) \frac{\partial}{\partial r_{3j}} v(\mathbf{r}_3) d\mathbf{r}_0 d\mathbf{r}_1 d\mathbf{r}_2 d\mathbf{r}_3.\end{aligned} \tag{16}$$

The second expression here is obtained via integration by parts. The gradient of $v(\mathbf{r})$ is zero everywhere except at the surface, where it has a contribution only from the component parallel to the surface normal:

$$\frac{\partial}{\partial r_i} v(\mathbf{r}) = \hat{\mathbf{e}}_i \cdot \nabla v(\mathbf{r}) = n_i(\mathbf{r}) \int_\Omega dS_1 \delta^3(\mathbf{r}_1 - \mathbf{r}), \tag{17}$$

where $\hat{\mathbf{e}}_i$ is a unit vector along the direction i and $n_i(\mathbf{r})$ is the ith component of the local outward normal vector $\hat{\mathbf{n}}(\mathbf{r})$. Therefore Eq. (16) can be reduced to a double surface integral, and the second-order velocity cumulant takes the form

$$\begin{aligned}u_{ij}^{(2)}(t_1, t_2) &= 2D_0 \delta_{ij} \delta(t_2 - t_1) \\ &\quad - \frac{D_0^2}{V} \int_\Omega n_i(\mathbf{r}_1) \psi(\mathbf{r}_2, \mathbf{r}_1, |t_2 - t_1|) n_j(\mathbf{r}_2) dS_1 dS_2.\end{aligned} \tag{18}$$

In obtaining Eq. (18) it was used that the bulk mean velocity, $\langle v_i(t) \rangle$, is zero for diffusion within any closed geometry. Eq. (18) can also be obtained by a perturbative account for the diffusion-sensitizing gradients in the Bloch–Torrey equation. This method is outlined in Appendix A, along with another method based directly on the diffusion equation. The first term in Eq. (18) comes from the case $t_2 - t_1 < \Delta t$, for which most spins do not sense the boundary but only the bulk medium. The second term is due to the boundary. It is equal to the average probability for molecules to travel between two surface points, while the surface orientation at these points defines the relevant component of the diffusion tensor. This, in particular, means that it is sufficient to know the diffusion propagator, ψ, at the pore surface in order to find any non-trivial diffusion effects.

3. Results

Application of Eq. (18) is illustrated by a calculation of the diffusion-weighted signal in three geometries, for which the diffusion propagator is known analytically: diffusion between two parallel planes (denoted below as a slab), within a cylinder and a sphere. Three different pulse sequences are considered. First, we focus on the two limiting cases of the Stejskal–Tanner pulse sequence, (Fig. 1): the limit of narrow pulses, $\delta \to 0$ and $g \to \infty$ such that $g\delta$ is constant (narrow pulse approximation), and the limit $\delta = \Delta = T_E/2$, where T_E is the echo time (Hahn spin–echo). Second, we consider a realistic measurement sequence: a spectroscopic PRESS volume selection dual spin–echo diffusion weighting sequence with eddy current compensation according to Ref. [9], Fig. 2. In the following, this sequence will be referred to as the PRESS sequence.

3.1. Slab

As the first example we consider ADC from a slab of a homogeneous medium restricted by two parallel, impermeable planes placed at $x = \pm R$, orthogonal to the x-axis. Diffusion in the y and z-direction is free, rendering the system effectively one-dimensional. The propagator for diffusion between two walls as an expansion in eigenfunctions is given in Appendix B. The second-order velocity cumulant is diagonal with the entries

$$u_{xx}^{(2)} = 2D_0\delta(t_2 - t_1) - \frac{D_0^2}{R}[\psi(R, R, t_2 - t_1) - \psi(-R, R, t_2 - t_1)] \tag{19}$$

$$= 2D_0\delta(t_2 - t_1) - \frac{2D_0^2}{R^2} \sum_{n=0}^{\infty} e^{-\left(n+\frac{1}{2}\right)^2 D_0 \pi^2 (t_2 - t_1)/R^2} \tag{20}$$

$$u_{yy}^{(2)} = u_{zz}^{(2)} = 2D_0\delta(t_2 - t_1). \tag{21}$$

In the limit of short times, $\sqrt{D_0\Delta} \ll R$, $\psi(-R, R)$ is negligible, and Eq. (19) agrees with the result in Ref. [5], Eq. 21, obtained using the method of mirror images.

By substitution of Eq. (20) into Eq. (8) we obtain an expression for the ADC along the x-axis which is valid for arbitrary pulse sequences. In the narrow pulse approximation, the ADC in the x-direction becomes

$$D = \frac{2D_0}{\pi^4\alpha^2} \sum_{n=0}^{\infty} \frac{1}{\left(n + \frac{1}{2}\right)^4} \left[1 - e^{-\left(n+\frac{1}{2}\right)^2 \pi^2 \alpha^2}\right], \tag{22}$$

where $\alpha = \sqrt{D_0\Delta}/R$. In the derivation, we used that $b = g^2\delta^2\Delta$ and $\sum_{n=0}^{\infty}(n + 1/2)^{-2} = \pi^2/2$. In the narrow pulse approximation, the exact signal is the Fourier transform of the diffusion propagator [10], also known as the characteristic function of the displacement

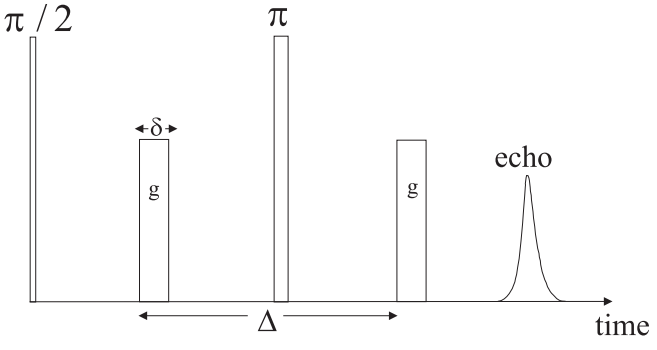

Fig. 1. Sequence of radio frequency and gradient pulses in a pulsed gradient spin–echo (Stejskal–Tanner) experiment. Δ is the duration between the two gradient pulses, δ the duration of each gradient pulse and g the amplitude of these pulses.

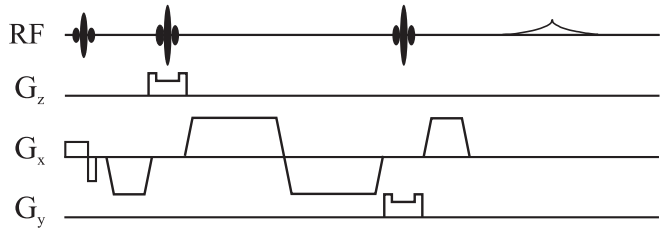

Fig. 2. Spectroscopic PRESS volume selection dual SE diffusion weighting sequence.

probability density function, and Eq. (22) coincides with the linear term in b in the expansion of the exact signal, given in Ref. [11].

For the Hahn spin–echo, the ADC takes the form

$$D = \frac{24D_0}{\pi^6\alpha^4}\sum_{n=0}^{\infty}\frac{1}{\left(n+\frac{1}{2}\right)^6}\left[1-\frac{3-4e^{-\frac{1}{2}\left(n+\frac{1}{2}\right)^2\pi^2\alpha^2}+e^{-\left(n+\frac{1}{2}\right)^2\pi^2\alpha^2}}{\left(n+\frac{1}{2}\right)^2\pi^2\alpha^2}\right], \quad (23)$$

where $\alpha = \sqrt{D_0 T_E}/R$ and $b = g^2 T_E^3/12$. Eq. (23) coincides with a similar expression in Ref. [7], obtained by calculating two volume integrals.

For the PRESS sequence we imported the exact shape of the gradient from the scanner and determined the ADC in the x-direction from Eqs. (8) and (20) numerically. The gradient was imported for a number of different b-values and different diffusion times T. To obtain a continuous ADC curve as a function of α, we used the gradient for one specific time and stretched it in such a way that the b-value remained the same when varying time. This is a good approximation to the exact gradient, although the time intervals between the two pairs of diffusion gradients in reality remain fixed. The apparent diffusion coefficients for the three different pulse sequences are shown in Fig. 3 as a function of α. The size of the slab is fixed at $R = 10\ \mu m$, the b-value at $b = 1.1\ ms/\mu m^2$ and the diffusion coefficient at $D_0 = 2\ \mu m^2/ms$. We used this diffusion coefficient as a good approximation to the value inside neuronal fibers, as discussed below in Section 4.2.

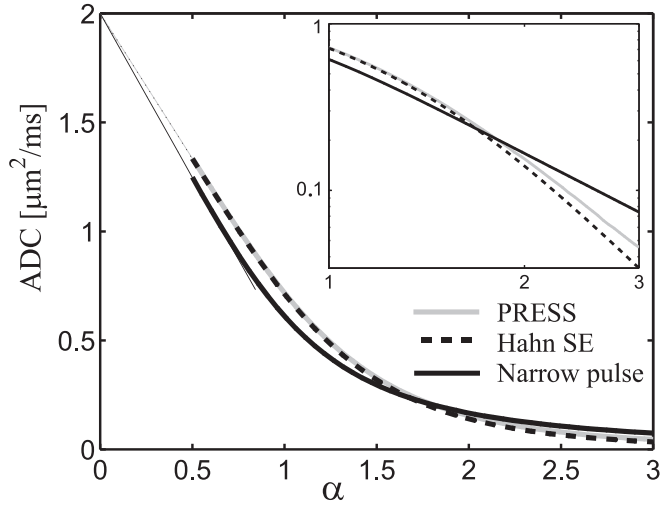

Fig. 3. The *ADC* as a function of α for diffusion between two reflecting walls. The thick dashed black line represents the Hahn spin–echo, the thick solid black line represents the narrow pulses and the thick solid grey line represents the PRESS pulse sequence. The curves are plotted for values of α between 0.5 and 3. The thin lines represent the short-time behavior for each of the pulse sequences, Eq. (1), using the same line style as above. The figure inserted in the right corner shows the same plots in double-log scales for $\alpha > 1$.

3.2. Cylinder

The infinite cylinder of radius R is effectively a two-dimensional system. The diffusion propagator is given in Appendix B.

The second-order velocity cumulant is diagonal as for the slab. The diagonal entries are given by

$$u_{xx}^{(2)} = u_{yy}^{(2)} = 2D_0\delta(t_2-t_1) - \frac{2D_0^2}{R^2}\sum_m \frac{\zeta_m^2}{\zeta_m^2-1}, e^{-D_0\zeta_m^2(t_2-t_1)/R^2} \quad (24)$$

$$u_{zz}^{(2)} = 2D_0\delta(t_2-t_1), \quad (25)$$

where ζ_m are the roots of the derivative of the Bessel function J_1'.

The gradient is now applied in a direction orthogonal to the cylinder axis, e.g., along x. Combining Eq. (8) with Eq. (24) yields

$$D = \frac{2D_0}{\alpha^2}\sum_m \frac{1}{\zeta_m^4-\zeta_m^2}(1-e^{-\zeta_m^2\alpha^2}) \quad (26)$$

for the narrow pulse approximation and

$$D = \frac{24D_0}{\alpha^4}\sum_m \frac{1}{\zeta_m^6-\zeta_m^4}\left(1-\frac{3-4e^{-\frac{1}{2}\zeta_m^2\alpha^2}+e^{-\zeta_m^2\alpha^2}}{\zeta_m^2\alpha^2}\right), \quad (27)$$

for the Hahn spin–echo. In obtaining Eqs. (26) and (27) it was used that $\sum_m(\zeta_m^2-1)^{-1} = 1/2$ [7,12]. Again the narrow pulse result, Eq. (26), is identical to the linear term in b in the expansion of the exact signal from Ref. [11], and the Hahn spin–echo result, Eq. (27), coincides with Ref. [7].

The apparent diffusion coefficient for the three pulse sequences is shown in Fig. 4 as a function of α, with parameters equal to those used for the slab.

3.3. Sphere

For the sphere, the second-order velocity cumulant is diagonal. The diagonal entries are equal and given by

$$u_{xx}^{(2)} = u_{yy}^{(2)} = u_{zz}^{(2)} = 2D_0\delta(t_2-t_1) - \frac{2D_0^2}{R^2}\sum_m \frac{\xi_m^2}{\xi_m^2-2}e^{-D_0\beta_m^2(t_2-t_1)/R^2}, \quad (28)$$

where ξ_m are the roots of the derivative of the spherical Bessel functions j_1' and R is the radius of the sphere.

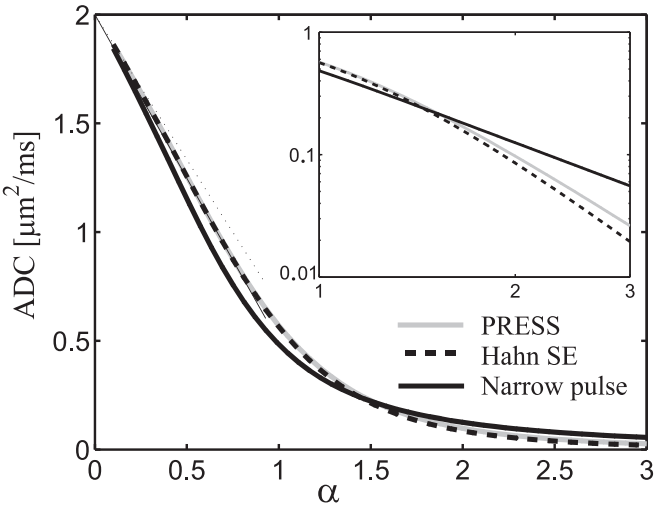

Fig. 4. The ADC as a function of α for diffusion in an infinite cylinder. The line style is the same as in Fig. 3. The short-time behavior (thin lines) is given by Eq. (1). The inserted figure shows the same plots in double-log scales.

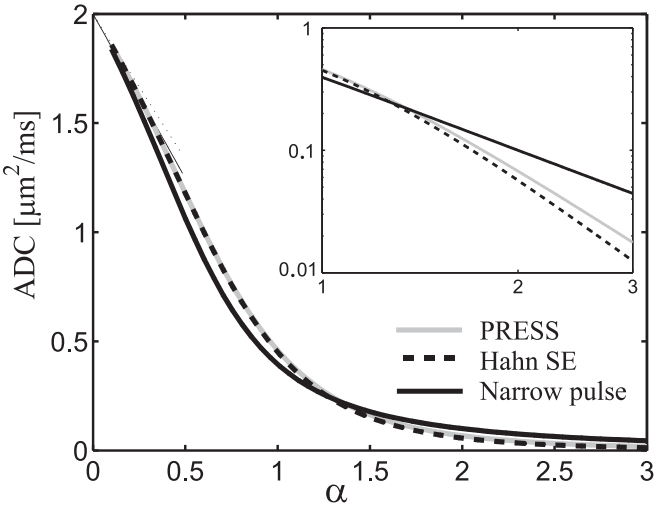

Fig. 5. The ADC as a function of α for diffusion in a sphere. The line style is the same as in Fig. 3. The short-time behavior (thin lines) is given by Eq. (1). The inserted figure shows the same plots in double-log scales.

The gradient is applied along the x-axis. Combining Eqs. (8) and (28) yields

$$D = \frac{2D_0}{\alpha^2}\sum_m \frac{1}{\xi_m^4 - 2\xi_m^2}\left(1 - e^{-\frac{\xi_m^2}{\xi_m}\alpha^2}\right) \tag{29}$$

for the narrow pulse approximation and

$$D = \frac{24D_0}{\alpha^4}\sum_m \frac{1}{\xi_m^6 - 2\xi_m^4}\left(1 - \frac{3 - 4e^{-\frac{1}{2}\xi_m^2\alpha^2} + e^{-\xi_m^2\alpha^2}}{\xi_m^2\alpha^2}\right), \tag{30}$$

for the Hahn spin–echo. Here we used the expression $\sum_m(\xi_m^2 - 2)^{-1} = 1/2$ [7,12]. Again the narrow pulse result, Eq. (26), coincides with the linear term in b in the expansion of the exact signal given in Ref. [11], and the Hahn spin–echo result, Eq. (27), coincides with Ref. [7].

For the PRESS sequence, the ADC in the x-direction is found by numerical integration of Eqs. (8), (28). In Fig. 5 it is shown as a function of α, together with ADC for the narrow pulse approximation and the Hahn spin–echo with parameters equal to those used for the slab and cylinder.

4. Discussion

The main result of this paper is stated in Eq. (18), which relates the second-order velocity cumulant to the diffusion propagator evaluated at the boundary. The velocity cumulant consists of a contribution from free diffusion in the bulk medium and a double surface integral of the diffusion propagator, ψ. This demonstrates that the second-order velocity cumulant is uniquely defined by the shape of the pore. The conventional expression for the ADC [7,2] includes the integral over the whole pore volume:

$$D = \frac{1}{2bV}\int_0^T dt_1\, dt_2 \int_V d\mathbf{r}_1\, d\mathbf{r}_2 x_1 x_2 \psi(\mathbf{r}_2, \mathbf{r}_1, t_2 - t_1) g(t_1) g(t_2). \tag{31}$$

For a given boundary condition, the diffusion propagator is uniquely defined via the solution to the diffusion equation. Hence Eq. (18) does not imply a reduction of the information content reflected in the ADC, but only expresses it in a condensed way.

The fact that the expression in Eq. (18) is reduced to a double surface integral compared to the double volume integral in Eq. (31) simplifies analytical calculation of the ADC, and reduces computation time in numerical simulations. The two representations are related via the diffusion equation and the partial volume integration (see Appendix A).

4.1. Dependence of ADC on pulse sequence and pore geometry

The apparent diffusion coefficient is shown as a function of α for the geometries and pulse sequences considered in Figs. 3–5. The α-range covered in the figures corresponds to diffusion times varying from 0 to 450 ms.

In the limiting case of $\alpha = \sqrt{D_0 T/R^2} \to 0$, the molecules do not encounter the restricting boundaries and therefore $D = D_0$. In the case of large α, ADC goes toward zero, as the molecules cannot explore distances larger than the size of the object that restricts their diffusion. Hence the mean square displacement ceases to grow with time.

For all three geometries, the ADC curves for the PRESS and Hahn spin–echo sequences are hardly distinguishable. The maximum difference between them occurs for $\alpha \approx 2$ and is close to 10^{-2} μm²/ms (corresponding to ~10%). The ADC for the narrow pulse approximation is clearly distinguishable from the other two pulse sequences, however, the largest difference, found for $0.5 < \alpha < 1$, is only ≈0.1 μm²/ms (corresponding to ~13%).

The low sensitivity of ADC to the details of the pulse sequence is fortunate for further investigation of diffusion-weighted MRI in terms of microstructure, as the practical advantages of clinical sequences can be combined with the theoretical convenience of the narrow pulse approximation and Hahn spin–echo, as far as the ADC is concerned.

The results presented in Figs. 3–5 agree well with the short-time behavior of the ADC, given by Eq. (1). For the narrow pulses and the Hahn spin–echo the coefficient c in Eq. (1) is given by

$$c_{\mathrm{NP}} = \frac{4}{3\sqrt{\pi}d} \tag{32}$$

and

$$c_{\mathrm{SE}} = \frac{32}{35\sqrt{2\pi}d}\left(2\sqrt{2} - 1\right), \tag{33}$$

respectively [1,3], where d is the spatial dimension. For diffusion between two walls, the coefficient takes the following form for an arbitrary pulse sequence:

$$c_{1d} = \frac{1}{2b\sqrt{\pi T}}\int_0^T dt_1 \int_0^T dt_2\, \frac{G(t_1)G(t_2)}{\sqrt{|t_2 - t_1|}}. \tag{34}$$

The substitution $t_2 = t_1 + y^2$ can be helpful for numerical calculations. The short-time ADC for diffusion in a slab deviates from the exact ADC with less than 1% up to $\alpha \approx 0.7$ for all three pulse sequences shown in Fig. 3. This extends the limit, $\alpha < 0.3$, found by Sukstanskii and colleagues, Ref. [13], below which the two regions adjacent to the walls can be considered independent. For the cylinder and the sphere, the short-time ADC is compared to the exact ADC for the narrow gradient pulses and the Hahn spin–echo sequence, resulting in deviations within 1% up to $\alpha \approx 0.2$ and $\alpha \approx 0.1$, respectively.

Fig. 6 shows the fractional anisotropy, FA, for the slab and cylinder as a function of α. FA is given by

$$\mathrm{FA} = \frac{\sqrt{3}}{\sqrt{2}}\frac{\sqrt{\sum_{i=1}^3(\lambda_i - \lambda)^2}}{\sqrt{\sum_{i=1}^3 \lambda_i^2}}, \tag{35}$$

where λ_i are the eigenvalues of the ADC tensor and λ is the mean diffusivity (one third of the trace of the ADC tensor).

For the cylinder, the FA is zero in the limit $\alpha \to 0$ (perfectly isotropic diffusion) and 1 in the limit $\alpha \to \infty$, which corresponds to an infinitely narrow cylinder. For diffusion between two planes FA is

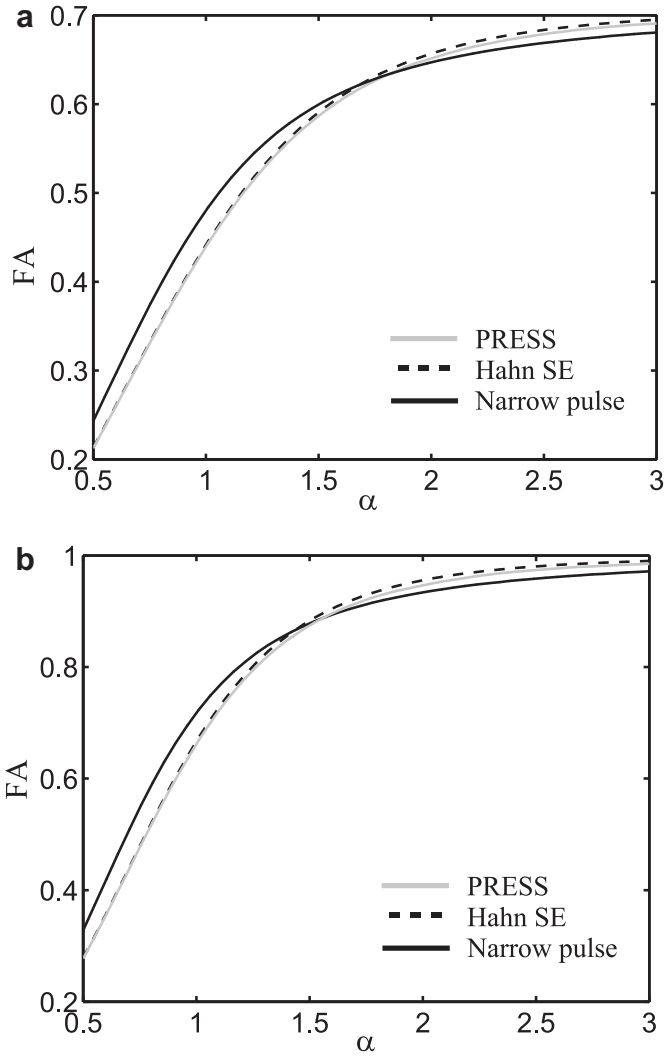

Fig. 6. Fractional anisotropy as a function of $\alpha \equiv \sqrt{D_0 T}/R$ for diffusion (a) between two walls and (b) in an infinite cylinder. The solid black line represents the narrow pulse approximation, the dashed black line represents the Hahn spin–echo and the solid grey line represents the PRESS pulse sequence.

also zero for $\alpha \to 0$ but $1/\sqrt{2}$ for $\alpha \to \infty$. These limits are seen in Fig. 6. The FA for the Hahn spin–echo and the PRESS sequence are nearly identical. The largest deviation between the two curves is found at $\alpha \approx 2$, corresponding to the time where the diffusion length of the spins equals the diameter of the objects. For the narrow pulse approximation, the limiting regimes mentioned above is reached later than for the other two pulse sequences. For the sphere, diffusion is perfectly isotropic and FA equals unity for all values of α.

4.2. Perspectives for the microstructural study of white matter

The infinitely long cylinder can be used as a reasonable model for fibers and dendrites [14–17]. We now consider the diffusion-weighted signal in the direction orthogonal to fibers and assume that it can be written as a sum of the intra- and extracellular signals, where both signal contributions are described by the cumulant expansion. Then the apparent diffusion coefficient can be found as

$$D = w_1 D_1 + w_2 D_2, \tag{36}$$

with w_1 and w_2 being the volume fractions of the intra- and extra-axonal compartments, respectively. Neglecting water in the myelin layers, which practically do not contribute to the signal due to the fast transverse relaxation, the normalized volume fractions are estimated as approximately $w_1 = 0.6$ and $w_2 = 0.4$ in frontal white matter in humans and in rat trigeminal nerve [18,19].

The results presented in Fig. 4 help to relate D_1 to the fiber size and the bulk diffusion coefficient inside the axons. Assuming that the ADC derived from the fiber signal is known with an uncertainty of 0.1 $\mu m^2/ms$, the fiber radius could be determined within 10–20% in a range of α-values from 0.3 to 1.7, with the best precision around $\alpha = 0.9$. For fibers with a radius of 10 μm this requirement means that the diffusion time should lie within the interval 5 to 150 ms, which is fulfilled in most experimental protocols.

For large values of α, the ADC-curve flattens out and becomes less sensitive to the radius. In the human corpus callosum, the fiber radius, R, varies between ~0.3 μm and ~5 μm, with $R = 1$ μm occurring most frequently, [20]. This radius is used in the following estimates. In order to be sensitive to this radius, the diffusion time in the experiment should be smaller than 1.5 ms, which is presently not achievable in scanners used in clinic settings. In Ref. [21], Does and colleagues experimentally obtained such short diffusion times in an animal scanner using oscillating gradients. In this paper they found that the "long diffusion time" limit, where the ADC becomes almost insensitive to α, starts around $\alpha \sim 2$—3, in agreement with the discussion above.

For a typical diffusion time of 80 ms, which we use in the estimations below, and a bulk diffusion coefficient of $D_0 = 2$ $\mu m^2/ms$ in the intraaxonal space [14,15,22,23], $\alpha \approx 13$. For such a large α-value, D_1 is negligible (Fig. 4) and the ADC measured orthogonal to the fibers is dominated by the extraaxonal space, according to Eq. (36). The precise value of the intraaxonal diffusion constant is thus irrelevant for diffusion in the transverse direction, but indispensable for understanding the diffusion in the direction parallel to the fibers.

This reduction in the number of free parameters enables an estimate of the extracellular diffusion coefficient in the direction orthogonal to the fibers, which at long times is described by the tortuosity, λ, defined through $D = D_0/\lambda^2$, where $D_0 = 3$ $\mu m^2/ms$ is the true diffusion constant of unrestricted water. We estimate the extraaxonal tortuosity in white matter using experimental data reported in Ref. [24]. The ADC was measured to be 2.0 $\mu m^2/ms$ parallel to myelinated fibers and 0.3 $\mu m^2/ms$ orthogonal to the fibers in corpus callosum for a diffusion time of 80 ms and an echo time of 112 ms.

The result for the extraaxonal tortuosity is $\lambda = 2.0$. However, to make a proper estimate of λ, the differences in the T_2 relaxation in the intra- and extracellular compartments should be accounted for when determining the volume fractions. Attempts have been made to find corresponding T_2 values by modelling the T_2 weighted signal with a three-pool model and associating the two largest T_2 values with the intra- and extracellular compartments [18,19]. For frontal white matter in children $T_{2,\text{intra}} = 40$ ms and $T_{2,\text{extra}} = 130$ ms has been measured [18]. Using these T_2 values we find $\lambda = 2.8$. The value of 2.8 is, however, not necessarily accurate for diffusion in human corpus callosum, since the T_2 values and volume fractions in frontal white matter might differ significantly from those in corpus callosum. Furthermore, the assignment of T_2 components, found from the three-pool model, to myelin, intra- and extracellular space lacks further independent validation. The extracellular tortuosity values can be compared to the tortuosity of 1.7 measured in rat corpus callosum [25,26]. Due to differences in cytoarchitecture across species, this number might differ in humans. This discussion demonstrates, that a better knowledge of the intra- and extracellular T_2 values, as well as the corresponding volume fractions, is needed for more reliable estimates of the tortuosity. This is in line with the conclusion from Ref. [27], stating that transverse relax-

ation should ultimately be accounted for in models of grey matter.

4.3. Limitations and extensions of the model

The expression for the ADC given by Eqs. (8) and (18) can be applied to an arbitrary pulse sequence and an arbitrary closed geometry with boundaries that are impermeable for diffusing spins. An open pore geometry, however, can be treated as the closed geometry with remote boundaries.

The effect of finite permeability of cellular membranes is not taken into account. It can be estimated in terms of a characteristic time, D_0/κ^2, where κ is the permeability, see Refs. [13,28] for a more detailed discussion. The membrane is well approximated as impermeable as long as this time is longer than the diffusion time. For a typical permeability of $10^{-2} - 10^{-1}$ μm/ms of biological membranes [28], this requirement is usually fulfilled in experiments.

The effect of surface relaxation has not been incorporated when deriving the expressions for the ADC. For $t \to 0$ it gives rise to terms which are proportional to time [2] and hence are smaller than the leading short-time term in the ADC of order $\sqrt{Dt}$. Surface relaxation is an important issue for NMR experiments in porous media. Its role in biological samples, however, is still poorly understood.

4.4. ADC and the diffusion-weighted signal

In the present paper, we have focused on the apparent diffusion coefficient, which is the most frequently used quantity to characterize diffusion and has proven to be useful for detecting cellular changes [29].

A standard estimate of the ADC is obtained from the diffusion-weighted signal, S, as the slope of $\ln S(b)$ for small b-values. However, as mentioned above, the ADC term, Eq. (2), is the lowest order term in the cumulant expansion of the signal and the quality of approximating the whole signal with the first term only should be considered in each particular case; the applicability depends on the desired accuracy as well as b-values and tissue properties. In a previous study [30], we considered theoretically the cumulant expansion for small α-values and found that for diffusion between two planes measured with the Stejskal–Tanner pulse sequence in the narrow pulse regime, two terms in the cumulant expansion are sufficient to describe the signal for practically relevant b-values. In Refs. [31,32] Stepišnik studied the cumulant expansion for large α-values, and concluded that higher order terms bring only small corrections to the Gaussian phase approximation, which is equivalent to keeping only the ADC term in the cumulant expansion.

The formalism developed in the present work can be applied beyond the ADC term to study higher order velocity cumulants as well. A more generally applicable approach is to calculate the exact signal using the matrix solutions to the Bloch–Torrey equation, as developed by Callaghan and Barzykin [33,34]. These formalisms can also be applied with an arbitrary gradient form; however, a complicated analytical structure with products of high-dimensional matrices may render this approach better suited for precise numerical computations than for analytical insight.

5. Conclusion

In this paper, we have considered the apparent diffusion coefficient (ADC) for an arbitrary closed geometry. For a given pulse sequence, the ADC can be determined from the second-order velocity cumulant, which we show to be expressible as a double surface integral of the probability to diffuse between two surface points (Eq. (18)). This demonstrates explicitly that the second-order velocity cumulant is uniquely defined by the shape of the restricting object. This insight simplifies analytical calculation of the ADC, and can reduce computation time of numerical simulations.

The applicability of Eq. (18) is demonstrated for diffusion within three geometries: a slab, a cylinder and a sphere. For each geometry the ADC was calculated for the Hahn spin–echo pulse sequence, the narrow pulse approximation of the Stejskal–Tanner pulse sequence and for a more complex pulse sequence with slice selection gradient and eddy current compensation (PRESS sequence) [9]. Only small differences were found between the ADCs for the three pulse sequences. In particular, the Hahn spin–echo and PRESS sequence gave almost identical results. This can simplify interpretation of experimental data across pulse sequences.

Finally we have discussed the possibility of gaining microscopic information of living tissue from the derived expressions for the ADC in simple geometries. By using cylinders to model neuronal fibers, we found that, for realistic diffusion times in human scanners, the ADC measured orthogonal to the fibers in the corpus callosum is strongly dominated by extraaxonal diffusion. Furthermore, estimation of biological parameters, such as tortuosity and fiber radius, depends significantly on the differences in the transverse relaxation in the intra- and extraaxonal compartments, of which present knowledge is limited.

Acknowledgments

We are grateful to the Danish National Research Foundation's Center of Functionally Integrative Neuroscience (A.F., S.N.J. and L.Ø.) and The Danish Medical Research Council (L.Ø.) for supporting this work. We are grateful to Niels Buhl for useful discussions.

Appendix A

An alternative way to obtain Eq. (18) is to solve the Bloch–Torrey equation perturbatively, with the amplitude of the diffusion-weighting gradient as the small parameter. This is achieved by expanding the Green's function, Ψ, of this equation as $\Psi = \Psi_0 + \Psi_1 + \Psi_2 + \ldots$, where Ψ_n is proportional to g^n and $\Psi_0 = \psi$. The signal to the nth order in g, S_n, can now be found by integrating the Greens' function,

$$S_n = \int \sum_{i=0}^{n} \Psi_i(\mathbf{r}, \mathbf{r}_0) \frac{\mathrm{d}\mathbf{r}\mathrm{d}\mathbf{r}_0}{V}. \tag{A1}$$

A non-trivial result is obtained in the second order:

$$\ln S_2 = -\frac{1}{2V} \int_0^T \mathrm{d}t_2 \int_0^T \mathrm{d}t_1 \int_V \mathrm{d}\mathbf{r}_1 \mathrm{d}\mathbf{r}_2 \mathbf{g}(t_1) \cdot \mathbf{r}_1 \times \psi(\mathbf{r}_2, \mathbf{r}_1, |t_2 - t_1|)\mathbf{g}(t_2) \cdot \mathbf{r}_2, \tag{A2}$$

which can be brought to the form of Eq. (8) by partial integration.

Instead of using the velocity operator defined in Section 2.2, the velocity autocorrelation function can also be found by differentiation of the position autocorrelation function

$$\langle v_i(t_1) v_j(t_2) \rangle = \frac{\mathrm{d}}{\mathrm{d}t_1} \frac{\mathrm{d}}{\mathrm{d}t_2} \langle r_i(t_1) r_j(t_2) \rangle. \tag{A3}$$

Consider the function f_{ij} defined for $t_1 < t_2$ by

$$f_{ij}(t_2 - t_1) \equiv \langle r_i(t_1) r_j(t_2) \rangle = \frac{1}{V} \int_V r_{1i} r_{2j} \psi(\mathbf{r}_2, \mathbf{r}_1, t_2 - t_1) \mathrm{d}\mathbf{r}_1 \mathrm{d}\mathbf{r}_2. \tag{A4}$$

Eq. (A3) is then written in the form

$$\langle v_i(t_1) v_j(t_2) \rangle = -\Theta(t_2 - t_1) \ddot{f}_{ij}(t_2 - t_1) - \Theta(t_1 - t_2) \ddot{f}_{ij}(t_1 - t_2) - 2\delta(t_2 - t_1) \dot{f}_{ij}(0), \tag{A5}$$

where Θ is the Heaviside step function and dots denote the time derivative. By replacing the time derivative of the diffusion propagator with $D_0\nabla^2\psi(\mathbf{r_2},\mathbf{r_1},t_2-t_1)$ according to the diffusion equation, Eq. (10), using Green's second theorem and the boundary condition, Eq. (12), $\ddot{f}_{ij}$ can be identified with the second term in Eq. (18) and $\dot{f}_{ij}(0)$ can be found by Gauss' theorem,

$$\dot{f}_{ij}(0) = -D_0\delta_{ij}. \tag{A6}$$

Using Eq. (A5), we finally retrieve Eq. (18).

Appendix B

Standard Sturm–Liouville theory allows the solution to partial differential equations to be expanded in orthogonal eigenfunctions determined by the relevant boundary conditions, see for example Ref. [35], chapt. 9.

For diffusion between parallel planes, the expansion in eigenfunctions for the diffusion propagator takes the form [10]

$$\begin{aligned}\psi(x,x_0,t_2-t_1) &= \frac{1}{2R}+\frac{1}{R}\sum_{n=1}^{\infty}\exp\left(-\frac{\xi_n^2 D_0(t_2-t_1)}{R^2}\right)\cos\left(\frac{\xi_n x}{R}\right)\cos\left(\frac{\xi_n x_0}{R}\right)\\ &\quad+\frac{1}{R}\sum_{n=0}^{\infty}\exp\left(-\frac{\zeta_n^2 D_0(t_2-t_1)}{R^2}\right)\sin\left(\frac{\zeta_n x}{R}\right)\sin\left(\frac{\zeta_n x_0}{R}\right),\end{aligned} \tag{A7}$$

where $t_1 < t_2$ and where the eigenvalues ξ_n and ζ_n are determined by $\sin(\xi_n)=0$ and $\cos(\zeta_n)=0$. In the y- and z-direction the diffusion propagator is Gaussian.

In polar coordinates (r,θ,z) the diffusion propagator for diffusion inside an infinite cylinder takes the form [11]

$$\begin{aligned}\psi(\mathbf{r_2},\mathbf{r_1},t_2-t_1) &= \frac{1}{\pi R^2}+\sum_{n>0}\sum_{m}\frac{2J_n(\zeta_{mn}r_1/R)J_n(\zeta_{mn}r_2/R)}{\pi R^2(1-n^2/\zeta_{mn}^2)(J_n(\zeta_{mn}))^2}\\ &\quad\times(\cos n\theta_1\cos n\theta_2+\sin n\theta_1\sin n\theta_2)\\ &\quad\times \mathrm{e}^{-D_0\zeta_{mn}^2(t_2-t_1)/R^2},\end{aligned} \tag{A8}$$

where J_n are the Bessel functions and ζ_{mn} is the mth root of J_n'. In the z-direction the diffusion propagator is Gaussian.

For the sphere, the diffusion propagator is found in spherical coordinates to be

$$\begin{aligned}\psi(\mathbf{r_2},\mathbf{r_1},t_2-t_1) &= \frac{1}{4\pi R^3}+\frac{1}{R^3}\sum_{n>0}\sum_{m}\frac{(2n+1)}{2\pi}\\ &\quad\times j_n(\xi_{mn}r_1/R)j_n(\xi_{mn}r_2/R)P_n(\cos\theta_1)P_n(\cos\theta_2)\\ &\quad\times(j_n^2(\xi_{mn})-j_{n-1}(\xi_{mn})j_{n+1}(\xi_{mn}))^{-1}\times\mathrm{e}^{-D_0\xi_{mn}^2(t_2-t_1)/R^2},\end{aligned} \tag{A9}$$

where j_n are the spherical Bessel functions and ξ_{mn} is the m'th root of j_n'.

References

[1] P. Mitra, P. Sen, L. Schwartz, P. Le Doussal, Diffusion propagator as a probe of the structure of porous media, Phys. Rev. Lett. 68 (1992) 3555–3558.
[2] P.P. Mitra, P.N. Sen, M. Schwartz, Short-time behaviour of the diffusion coefficient as a geometrical probe of porous media, Phys. Rev. B 47 (14) (1993) 8565–8574.
[3] T. de Swiet, P. Sen, Decay of nuclear magnetization by bounded diffusion in a constant field gradient, J. Chem. Phys. 100 (8) (1994) 5587–5604.
[4] P. Sen, Time-dependent diffusion coefficient as a probe of geometry, Concepts Magn. Reson. A 23A (1) (2004) 1–21.
[5] A.F. Frøhlich, L. Østergaard, V.G. Kiselev, Effect of impermeable interfaces on apparent diffusion coefficient in heterogeneous media, Appl. Magn. Reson. 29 (2005) 123–137.
[6] P. Callaghan, Principles of Nuclear Magnetic Resonance Microscopy, Oxford University Press, 1991 [chapter 6].
[7] C.H. Neuman, Spin–echo of spins diffusing in a bounded medium, J. Chem. Phys. 60 (1974) 4508–4511.
[8] P. Kingsley, Introduction to diffusion tensor imaging mathematics: part III. Tensor calculation, noise, simulations, and optimization, Concepts Magn. Reson. A 28A (2) (2006) 155–179.
[9] T. Reese, O. Heid, R. Weisskoff, V. Wedeen, Reduction of eddy-current-induced distortion in diffusion MRI using a twice-refocused spin–echo, Magn. Reson. Med. 49 (2003) 177–182.
[10] J.E. Tanner, E.O. Stejskal, Restricted self-diffusion of protons in colloidal systems by pulsed-gradient, spin–echo method, J. Chem. Phys. 49 (1968) 1768–1777.
[11] P. Callaghan, Pulsed-gradient spin–echo NMR for planar, cylindrical and spherical pores under conditions of wall relaxation, J. Magn. Reson. 113 (1995) 53–59.
[12] G. Watson, Theory of Bessel Functions, Cambridge, UP, Cambridge, England, 1962, pp. 576–581.
[13] A.L. Sukstanskii, J.J.H. Ackerman, D.A. Yablonskiy, Effects of barrier-induced nuclear spin magnetization inhomogeneities on diffusion-attenuated MR signal, Magn. Reson. Med. 50 (2003) 735–742.
[14] S. Jespersen, C. Kroenke, L. Østergaard, J. Ackerman, D. Yablonskiy, Modeling dendrite density from magnetic resonance diffusion measurements, NeuroImage 34 (2007) 1473–1486.
[15] C. Kroenke, J. Ackerman, D. Yablonskiy, On the nature of the NAA diffusion attenuated MR signal in the central nervous system, Magn. Reson. Med. 52 (2004) 1052–1059.
[16] Y. Assaf, R. Freidlin, G. Gustavo, K. Rohde, P. Basser, New modeling and experimental framework to characterize hindered and restricted water diffusion in brain white matter, Magn. Reson. Med. 52 (2004) 965–978.
[17] P. Sen, P. Basser, Modeling diffusion in white matter in the brain: a composite porous medium, Magn. Reson. Imaging 23 (2005) 215–220.
[18] J. Lancaster, T. Andrews, L. Hardies, S. Dodd, P. Fox, Three-pool model of white matter, J. Magn. Reson. Imaging 17 (2003) 1–10.
[19] M. Does, J. Gore, Compartmental study of T1 and T2 in rat brain and trigeminal nerve in vivo, Magn. Reson. Med. 47 (2002) 274–283.
[20] F. Aboitiz, A. Scheibel, R. Fishe, E. Zaidel, Fiber composition of the human corpus callosum, Brain Res. 598 (1992) 143–153.
[21] M. Does, E. Parsons, J. Gore, Oscillating gradient measurements of water diffusion in normal and globally ischemic rat brain, Magn. Reson. Med. 49 (2003) 206–215.
[22] G. Stainisz, Diffusion MR in biological systems: tissue compartments and exchange, Isr. J. Chem. 43 (2003) 33–44.
[23] C. Beaulieu, P. Allen, Water diffusion in the giant axon of the squid: implications for diffusion-weighted MRI of the nervous system, Magn. Reson. Med. 32 (1994) 579–583.
[24] V. Kiselev, K. Ill'yasov, Diffusion-weighted signal in white matter: what is behind the b-factor dependence? in: Proceedings of the 16th Annual Meeting of ISMRM, Toronto, No. 4913, 2008.
[25] I. Vorsek, E. Sykova, Evolution of anisotropic diffusion in the developing rat corpus callosum, J. Neurophysiol. 78 (1997) 912.
[26] C. Nicholson, E. Sykova, Extracellular space structure revealed by diffusion analysis, Trends Neurosci. 21 (1998) 207–215.
[27] P. Vestergaard-Poulsen, B. Hansen, L. Østergaard, R. Jakobsen, Micro-structural changes in ischemic cortical gray matter predicted by a model of diffusion-weighted MRI, J. Magn. Reson. Imaging 26 (2007) 529–540.
[28] A.L. Sukstanskii, D.A. Yablonskiy, J.J.H. Ackerman, Effects of permeable boundaries on the diffusion-attenuated MR signal: insight from a one-dimensional model, J. Magn. Reson. 170 (2004) 56–66.
[29] P. Tofts, Quantitative MRI of the Bra, in: Measuring Changes Caused by Disease, John Wiley & Sons, Ltd., 2003.
[30] A. Frøhlich, L. Østergaard, V. Kiselev, Effect of impermeable boundaries on diffusion-attenuated MR signal, J. Magn. Reson. 179 (2006) 223–233.
[31] J. Stepišnik, Averaged propagator of restricted motion from the Gaussian approximation of spin–echo, Physica B 344 (2004) 214–223.
[32] J. Stepišnik, Validity limits of the Gaussian approximation in cumulant expansion for diffusion attenuation of spin–echo, Physica B 270 (1999) 110–117.
[33] P. Callaghan, A simple matrix formalism for spin–echo analysis of restricted diffusion under generalized gradient waveforms, J. Magn. Reson. 129 (1997) 74–84.
[34] A. Barzykin, Theory of spin–echo in restricted geometries under a step-wise gradient pulse sequence, J. Magn. Reson. 139 (1999) 342–353.
[35] G. Arfken, H. Weber, Mathematical Methods for Physicists, Academic Press, Harcourt, 2001 [chapter 9].